Li *et al.*
Chinese Journal of Mechanical Engineering (2022) 35:70
https://doi.org/10.1186/s10033-022-00724-1

Chinese Journal of Mechanical Engineering

ORIGINAL ARTICLE

Open Access

Vibration Characteristics of Rotor System with Loose Disc Caused by the Insufficient Interference Force

Zhinong Li[1,2*], Fang Qiao[1], Wenxiu Lu[3], Jie Liu[1], Dong Wang[4] and Fulei Chu[3]

Abstract

The rotating parts looseness is one of the common failures in rotating machinery. The current researches of looseness fault mainly focus on non-rotating components. However, the looseness fault of disc-shaft system, which is the main work part in the rotor system, is almost ignored. Here, a dynamic model of the rotor system with loose disc caused by the insufficient interference force is proposed based on the contact model of disc-shaft system with the microscopic surface topography, the vibration characteristics of the system are analyzed and discussed by the number simulation, and verified by the experiment. The results show that the speed of the shaft, the contact stiffness, the clearance between the disc and shaft, the damping of the disc and the rotational damping have an influence on the rotation state of the disc. When the rotation speed of the disc and the shaft are same, the collision frequency is mainly composed of one frequency multiplication component and very weak high frequency multiplication components. When the rotation speed of the disc and the shaft is close, the vibration of the disc occurs a beat vibration phenomenon in the horizontal direction. Simultaneously, a periodical similar beat vibration phenomenon also occurs in the waveform of the disc-shaft displacement difference. The collision frequency is mainly composed of a low frequency and a weak high frequency component. When the rotation speed of the disc and the shaft has great difference, the collision frequency is mainly composed of one frequency multiplication, a few weak high frequency multiplication components and a few low frequency multiplication component. With the reduction of the relative speed of the disc, the trajectory of the disc changes from circle-shape to inner eight-shape, and then to circle-shape. In the inner eight-shape, the inner ring first gradually becomes smaller and then gradually becomes larger, and the outer ring is still getting smaller. The obtained research results in this paper has important theoretical value for the diagnosis of the rotor system with the loose disc.

Keywords: Rotor system with loose disc, Rotor dynamics, Nonlinear dynamic characteristic, Nonlinear vibration, Insufficient interference force, Fault diagnosis

1 Introduction

Looseness fault of rotating parts, which is one of the common failures in the rotor system, has a serious influence on the normal operation of the rotor system, and leads to the reduction of mechanical power, or even machine malfunction. Generally, mechanical looseness includes pedestal looseness, base looseness and so on. For a double-disc single-span rotor system with pedestal looseness fault, Ma et al. [1] used three dimensional spectrums and shaft center trajectory to analyze the influence of no loose bolt stiffness, looseness gap, and rotational speed on the dynamic characteristics of the rotor system. Sun et al. [2] proposed a finite element model which can characterize complex structures, and verified the effectiveness of the proposed model by

*Correspondence: lizhinong@tsinghua.org.cn

[1] Key Laboratory of Nondestructive Testing, Ministry of Education, Nanchang Hangkong University, Nanchang 330063, China
Full list of author information is available at the end of the article

comparing critical speed and vibration mode. Zhang et al. [3] proposed a rotor model with nonlinear oil film force, and solved this mode by the numerical method of Runge-Kutta, and obtained frequency characteristics of the rotor system. Lu et al. [4] proposed a coupling model of the rotor system with looseness and rub-impact faults, and discussed the influence of the looseness stiffness and the clearance between rotor and stator on the dynamic characteristics of the rotor system based on the nonlinear finite element method and the contact theory. Based on nonlinearity measure, Mian et al. [5] proposed an evaluation method of the pedestal looseness in bearing-rotor system with piecewise-linear stiffness, damping and nonlinear elastic force under constant rotational speed at constant speed. In Ref. [6–9], the corresponding model was proposed, and the dynamic characteristics of the proposed model were analyzed. Liu [10] proposed a dynamic model of looseness-rubbing coupling fault in the rotor-bearing system with dual-disk and three-support. Wang [11] proposed a model of rotor-support-casing in the rotor system with support looseness fault. Yu [12] proposed a dynamic model of rotor-bearing system with loose support. Chen [13] proposed a dynamics model in a rotor-ball bearing-stator coupling system with rotor unbalance-loose coupling fault. For the complex movement of a single loose bearing pedestal rotor-bearing system, Zhang [14] proposed a nonlinear non-steady oil-film force model with short bearings. Cao et al. [15] proposed a nonlinear dynamic equation of rotor-bearing system with looseness fault between the pedestal and the casing. Xu et al. [16] proposed a dynamics model of dual rotor system with loose bearing pedestal based on the dual rotor structure of experiment rig. Yang et al. [17] analyzed the vibration features of the rotor system with respect to the effects of geometrical nonlinearity, rotor-stator rub and pedestal looseness, and revealed the change rules of resonant characteristic and rub region under different loose stiffness. Cao et al. [18] proposed a vibration differential equation with piecewise-linear stiffness by considering the system with one-side support looseness and the rotor with unbalanced extraneous exciting force. Cao et al. [19] proposed a dynamic model of rotor-bearing-pedestal system to investigate the vibration characteristics and stability due to fit clearance.

However, the above researches ignore the looseness fault in the disc-shaft system. Because the working environment of the disc in the rotor system is complex, and the working time is also long, the looseness of the disc-shaft easily occurs. When the interference between the disc and shaft is insufficient, the relative sliding of disc-shaft will be easily caused. This relative sliding has an influence on the dynamic characteristics of the rotor system with a loose disc. At present, some progress has been made in the looseness of rotating parts of rotor system [20–25]. Behzad [20, 21] proposed the model of the looseness of disc-shaft system with large clearance based on the hypothesis that the rotating speed of the disc is constant, and the disc and the shaft are always in contact. However this model ignored the collision and friction of disc-shaft, and assumed that the disc and the shaft rotated at the same speed. Obviously, the engineering practice does not meet these requirements. In practice, the disc-shaft looseness in the rotor system generally also occurs when the clearance is small, even no clearance [22]. In our works [23, 24], a dynamic model of rotor system with the clearance between the shaft and the disc is proposed in Ref. [23],and a rotor system model with disc-shaft looseness with non-steady-state oil film force is proposed in Ref. [24]. Wei [25, 26] studied the disc-shaft looseness fault in rotor system caused by the excessive speed of the shaft. However these research results in disc-shaft system do not consider the influence of the disc-shaft looseness fault on the motion state of the rotor system with the insufficient interference force.

Therefore, the motion differential equations of the rotor system with loose disc caused by the insufficient interference force is proposed based on the contact model of the disc-shaft system with the microscopic surface morphology, and the numerical simulation and experiment test have been completed. The influence factors of the motion state of the disc, the vibration characteristics of the disc, the variation of the displacement difference of disc-shaft, and the trajectory of the disc. These obtained outcomes provide theoretical support for the fault diagnosis of the disc-shaft system with slight loose disc in engineering practice.

2 Mathematical Model

2.1 Contact Model of Disc-Shaft System with the Microscopic Surface Morphology

Figure 1 is a schematic diagram of disc-shaft contact [27]. In Figure 1, the outer ring represents the reference plane of the inner diameter of the disc and the inner ring

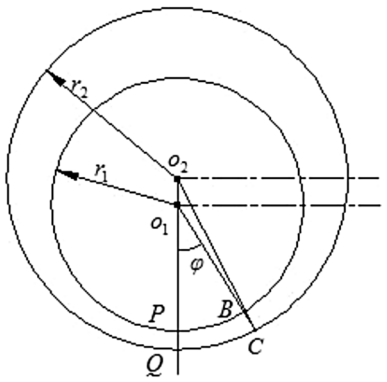

Figure 1 The contact model in disc-shaft system

represents the cylindrical surface of the outer diameter of the shaft. The coordinates of the center of the shaft, which is represented by o_1, is the point (x_1, y_1). The symbol r_1 is the radius of the shaft. The coordinates of the center of the disc, which represented by o_2, is the point (x_2,y_2). The symbol r_2 is the radius of the disc. The extension line of o_1o_2 intersects with the shaft and the disc at point $\boldsymbol{P}$ and point $\boldsymbol{Q}$ respectively. The line o_1Q rotated around the center of the shaft by an angle, which is represented by ϕ counterclockwise, and intersects with the shaft and the disc at points $\boldsymbol{B}$ and $\boldsymbol{C}$ respectively.

In the triangle Δo_1o_2C, the line $\overline{o_1o_2}$ is the relative distance $\boldsymbol{r}$ of disc-shaft, and $\overline{o_2C} = r_2$, According to cosine theorem, o_2C can be written as

$$\overline{o_2C}^2 = \overline{o_1o_2}^2 + \overline{o_1C}^2 - 2\overline{o_1o_2}\,\overline{o_1C}\cos\angle o_1o_2C. \quad (1)$$

Due to $\cos\angle o_2o_1C = -\cos\varphi$, Eq. (1) can be simplified as

$$r_2^2 = r^2 + \overline{o_1C}^2 + 2r\overline{o_1C}\cos\phi. \quad (2)$$

Then, at any angle ϕ, the clearance between the disc and shaft is as follows

$$\Delta d(\phi) = \overline{o_1C} - r_1 = \sqrt{r_2^2 - r^2\sin^2\phi} - r\cos\phi - r_1. \quad (3)$$

When the height of micro-convex, which is represented by z, is higher than the clearance between the disc and shaft, which is represented by $\Delta d(\phi)$, The normal force generated by the micro-convex can be obtained [24]

$$\Delta F = 4E'\gamma^{1/2}(z - \Delta d(\varphi))^{3/2}\Big/3, \quad (4)$$

$$1/\gamma = 1/\gamma_1 + 1/\gamma_2, \quad (5)$$

$$1/E' = 1/E_1 + 1/E_2, \quad (6)$$

where γ_1 is the radius of the disc, γ_2 is the radius of the shaft, γ is the radius of the micro-convex, E_1 is the elastic modulus of the disc, E_2 is the elastic modulus of the shaft, and E is the elastic modulus of the micro-convex. Suppose that the normal distribution function of z on the contact surface is $\phi(z)$, the mean of normal force generated by a single micro-convex at any angle φ is expressed as

$$\Delta\overline{F}(\varphi) = \int_{\Delta d(\varphi)}^{\infty} \Delta F\phi(z)\mathrm{d}z. \quad (7)$$

Let η is the density of the micro-convex, $r_1d(\varphi)$ is the length of the micro-convex, then the number of micro-convex is $\eta l r_1 \mathrm{d}\varphi$ on the micro-area segment with a width of l. The total force on the entire contact surface can be obtained by integrating Eq. (7)

$$\begin{aligned} F &= \int_0^{2\pi} \Delta\overline{F}\,\mathrm{d}\varphi \\ &= 4/3 l\eta r_1 E'\gamma^{1/2}\int_0^{2\pi}\int_{\Delta d(\varphi)}^{\infty}[z - \Delta d(\varphi)]\phi(z)\mathrm{d}z\mathrm{d}\varphi. \end{aligned} \quad (8)$$

Since the contact force is symmetric with respect to o_1o_2, Eq. (8) can be simplified as follows

$$F = \frac{8}{3} l\eta r_1 E'\gamma^{1/2}\int_0^{\pi}\int_{\Delta d(\varphi)}^{\infty}[z - \Delta d(\varphi)]\phi(z)\mathrm{d}z\mathrm{d}\varphi. \quad (9)$$

The radial force generated by a single micro-convex at any angle ϕ is $\Delta F_r = \Delta F\cos\varphi$, then the mean of radial force is $\Delta\overline{F_r}(\varphi) = \Delta\overline{F(\varphi)}\cos\varphi$. Therefore, the total radial force generated over the entire circumference can be expressed as follows

$$F_r = \frac{8}{3} l\eta r_1 E'\gamma^{1/2}\int_0^{\pi}\int_{\Delta d(\varphi)}^{\infty}[z - d(\varphi)]\phi(z)\cos\varphi\mathrm{d}z\mathrm{d}\varphi. \quad (10)$$

Suppose that the contact of each micro-convex meets to the conditions of friction law of Coulomb in the process of contact of disc-shaft, let μ is the friction coefficient at the contact point, and $\Delta\omega = \omega_1 - \omega_2$, where ω_1 is the rotation speed of the disc, ω_2 is the speed of the shaft. Then the tangential force generated by a single micro-convex at any angle φ is $\Delta F_t = \mathrm{sgn}(\Delta\omega)\Delta F\cos\varphi$, then the mean of the tangential force is $\Delta\overline{F_t}(\varphi) = \mathrm{sgn}(\Delta\omega)\Delta\overline{F}(\varphi)\cos\varphi$. the total tangential force generated over the entire circumference can be expressed as

$$F_t = \mathrm{sgn}(\Delta\omega)\frac{8}{3}\mu l\eta r_1 E'\gamma^{1/2}\int_0^{\pi}\int_{\Delta d(\varphi)}^{\infty}[z - \Delta d(\varphi)]\phi(z)\cos\varphi\mathrm{d}z\mathrm{d}\varphi, \quad (11)$$

where $\mathrm{sgn}(\Delta\omega)$ is the step function, which is expressed as

$$\mathrm{sgn}(\Delta\omega) = \begin{cases} 1, & \Delta\omega > 0, \\ 0, & \Delta\omega = 0, \\ -1, & \Delta\omega < 0. \end{cases} \quad (12)$$

The frictional force F_f generated by the entire contact surface of disc-shaft can be expressed as follows:

$$F_f = \mathrm{sgn}(\Delta\omega)\mu F. \quad (13)$$

The components of the force from the disc on the shaft in two coordinate directions are respectively expressed as follows.

$$\begin{Bmatrix} F_x \\ F_y \end{Bmatrix} = -\frac{1}{r}\begin{bmatrix} F_r & -F_t \\ -F_t & F_r \end{bmatrix}\begin{Bmatrix} x_1 - x_2 \\ y_1 - y_2 \end{Bmatrix}. \tag{14}$$

2.2 Motion Equations of the Rotor System with Loose Disc

Figure 2 shows a rotor system with concentrated mass and rigid support. This system is composed of a rotor and a loose disc. From Ref. [20], the influence of gyroscopic effect on the dynamic response of the system is very little, for simplicity, the gyroscopic effect is ignored. The dynamic response of the rotor system can be obtained by integrating the equation of motion.

The vibration equation of the shaft is expressed as follows

$$\begin{cases} m_1\ddot{x}_1 + c_1\dot{x}_1 + kx_1 = m_1e_1\omega^2\cos(\omega t) + f_x, \\ m_1\ddot{y}_1 + c_1\dot{y}_1 + ky_1 = m_1e_1\omega^2\sin(\omega t) - m_1g + f_y, \end{cases} \tag{15}$$

where m_1, c_1 and k are the mass, damping coefficient and stiffness coefficient of the shaft respectively, e_1 and ω are the eccentric distance and the rotation speed of the shaft respectively. f_x and f_y are the components of the force from the disc on the shaft in the x-direction and the y-direction respectively.

The vibration equations of the disc are is expressed as follows

$$\begin{cases} m_2\ddot{x}_2 + c_2\dot{x}_2 \\ = m_2e_2\dot{\theta}^2\cos\theta + m_2e_2\ddot{\theta}\sin\theta - f_x, \\ m_2\ddot{y}_2 + c_2\dot{y}_2 \\ = m_2e_2\dot{\theta}^2\sin\theta - m_2e_2\ddot{\theta}\cos\theta - m_2g - f_y, \end{cases} \tag{16}$$

where m_2 is the mass of the disc , c_2 is the vibration damping coefficient of the disc, e_2 is the eccentric distance of the disc.

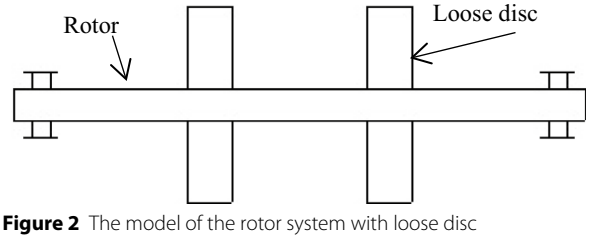

Figure 2 The model of the rotor system with loose disc

The rotational vibration equation of the disc is expressed as follows

$$j\ddot{\theta} + c_3\dot{\theta}^2 = f_tr_2 - m_2ge_2\cos\theta, \tag{17}$$

where j is the moment of inertia of the disc, c_3 is the rotational damping coefficient of the disc.

For the convenience of calculation and analysis, dimensionless to the equations [15–17], The dimensionless equation of motion can be written as

$$\begin{cases} \ddot{X}_1 = E_1\cos\tau + \frac{F_x}{\Omega^2} - \frac{\xi_1}{\Omega}\dot{X}_1 - \frac{K}{\Omega^2}X_1, \\ \ddot{Y}_1 = E_1\sin\tau - \frac{G}{\Omega^2} + \frac{F_y}{\Omega^2} - \frac{\xi_1}{\Omega}\dot{Y}_1 - \frac{k}{\Omega^2}Y_1, \\ \ddot{X}_2 = E_2\dot{\theta}^2\cos\theta + E_2\ddot{\theta}\sin\theta - \frac{F_x}{s\Omega^2} - \frac{\xi_2}{S\Omega}\dot{X}_2, \\ \ddot{Y}_2 = E_2\dot{\theta}^2\sin\theta - E_2\ddot{\theta}\cos\theta - \frac{F_y}{s\Omega^2} - \frac{\xi_2}{S\Omega}\dot{Y}_2 - \frac{G}{\Omega^2}, \\ \ddot{\theta} = F_tR^2\frac{1}{j\Omega^2} - SG\frac{1}{j\Omega^2}E_2\cos\theta - \frac{\xi_3}{j}\dot{\theta}^2, \end{cases} \tag{18}$$

where $\tau{=}\omega t$, $X_i{=}x_i/\sigma$, $Y_i{=}y_i/\sigma$, $\dot{X}_i{=}\mathrm{d}x_i/\mathrm{d}\tau$, $\dot{Y}_i{=}\mathrm{d}y_i/\mathrm{d}\tau$, $\ddot{X}_i{=}\mathrm{d}\dot{X}_i/\mathrm{d}\tau$, $\ddot{Y}_i{=}\mathrm{d}\dot{Y}_i/\mathrm{d}\tau$, $i{=}1{,}2$, $\omega_0 = \sqrt{k/(m_1+m_2)}$, $\Omega{=}\omega/\omega_0$, $E_1{=}e_1/\sigma$, $E_2{=}e_2/\sigma$, $\xi_1{=}c_1/m_1\omega_0$, $\xi_2{=}c_2/m_2\omega_0$, $\xi_3{=}c_3/m_3\sigma_2$, $K{=}k/m_1{\omega_0}^2$, $G{=}g/{\omega_0}^2\sigma$, $F_x{=}f_x/m_1{\omega_0}^2\sigma$, $F_y{=}f_y/m_1{\omega_0}^2\sigma$, $J{=}j/m_1\sigma_2$, $S{=}m_2/m_1$, $C{=}4/3l\eta r_1E'\sigma\sqrt{2\sigma\gamma/\pi}$. σ is the root mean square of the micro-convex distribution on contact surface of disc-shaft.

Due to the nonlinear of Eq. (18), its analytical solution is hardly obtained. Here the fourth-order Runge-Kutta [28–30] method is used to solve Eq. (18). In order to ensure the convergence of the solution and reduce the calculation error, the time step of the solution is set to $\pi/640$.

3 Numerical Analysis

In this model, the parameters is $\omega_0 = 500$, $E_1 = 1$, $E_2 = 4$, $G = 98/25$, $s = 1/3$, $J = 1/3 \times 10^7$, $\sigma = 10^{-5}$, the initial condition is that the disc is stationary.

3.1 Analysis of Motion State of the Disc

When the disc-shaft looseness fault occurs, the speed of the disc is no longer the same as speed of the shaft, and the motion state will inevitably change, this is also the unique characteristic of this fault. From Eqs. (10), (11), (13) and (18), the speed of the shaft Ω, contact stiffness C, clearance H, damping of the disc ξ_2 and rotational damping ξ_3 have an influence on the motion characteristics of the disc-shaft system. Therefore, the motion state of the disc is discussed mainly from the above several factors.

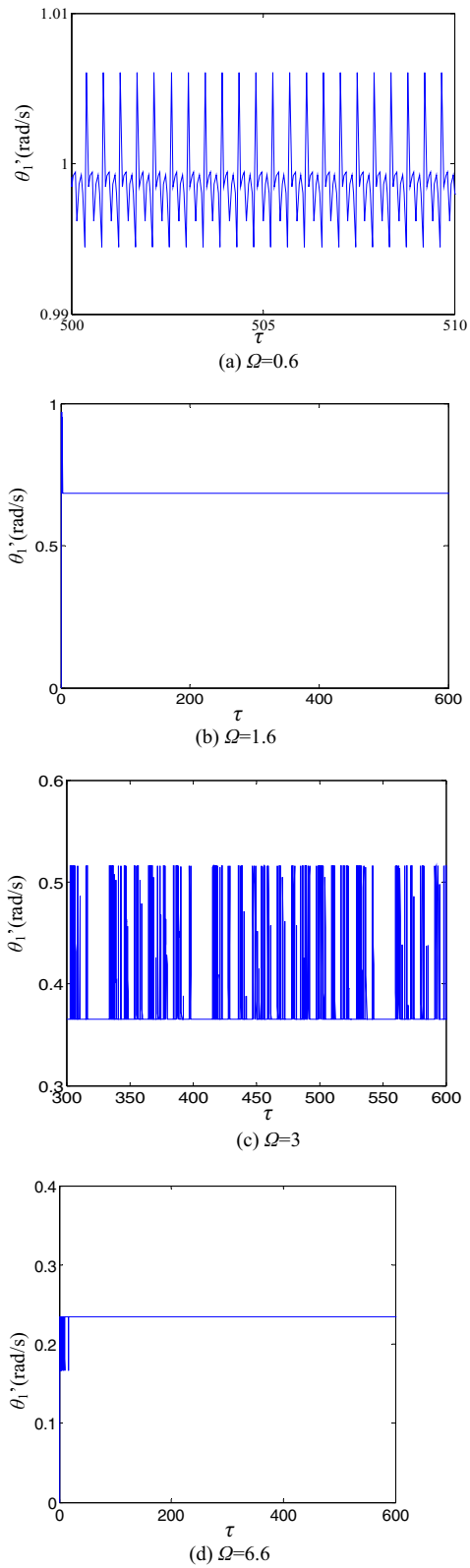

Figure 3 Change of θ_1' under the different Ω

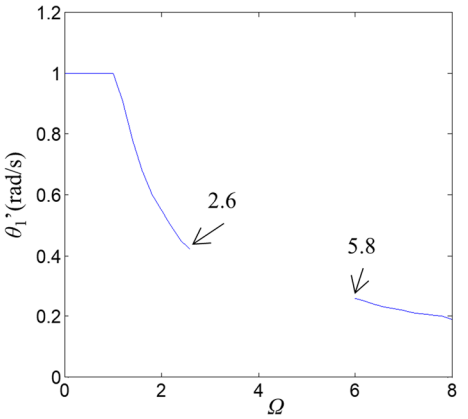

Figure 4 Change of θ_1' with Ω (The unmarked part indicates that θ_1' is in a surge state)

3.1.1 Influence of Shaft Speed

The change of relative speed of the disc θ_1' at different rotation speed of the shaft Ω is shown in Figure 3. The change of relative speed of the disc θ_1' with speed of the shaft Ω is shown in Figure 4. From Figure 3a, when $\Omega \leq 1$, the shaft speed of the disc is basically the same as that of the shaft. From Figure 3b, when $1 < \Omega \leq 2.6$, The disc is no longer at the same speed as the shaft, θ_1' decreases with the increase of Ω. From Figure 3c, when $2.6 < \Omega \leq 5.8$, the rotation speed of the disc is no longer stable and in a surge state. From Figure 3d, when $5.8 < \Omega$, the rotation speed of the disc returns to a stable state again, and the relative speed of the disc θ_1' continues to decrease with the increase of Ω. From Figure 4, when Ω is low, the disc and the shaft basically rotate at the same speed. With the increasing of Ω, θ_1' decreases gradually.

3.1.2 Influence of the Contact Stiffness of Disc-Shaft

Due to the contact stiffness of disc-shaft $C = 4/3l\eta r_1 E' \sigma \sqrt{2\sigma\gamma/\pi}$, i.e., there is a linear relationship between C and the contact stiffness of disc-shaft. Therefore, the influence of the elastic modulus on the motion state of the disc is known by discussing the influence of C on the motion state of the disc. Figure 5 is the change of relative speed of the disc θ_1' under the different C.

When $C \leq 4 \times 10^6$ N/m, θ_1' gradually increased with the increase of C, which is seen in Figure 5a. When 4×10^6 N/m $< C \leq 6 \times 10^7$ N/m, the rotational speed of the disc is in the state of surge, and θ_1' gradually increases with the increases of C, which is seen in Figure 5b. When 6×10^7 N/m $< C \leq 3 \times 10^8$ N/m, the rotation speed of the disc recovers to the stable state again, and

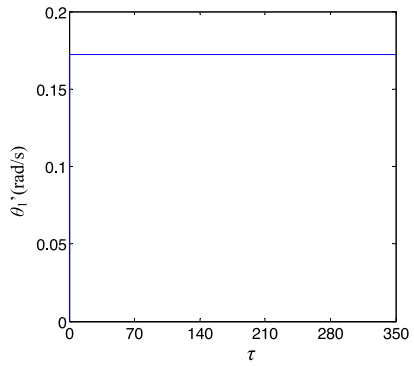

(a) $C = 4\times10^6$ N

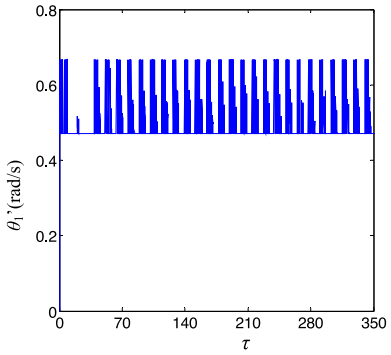

(b) $C=6\times10^7$ N

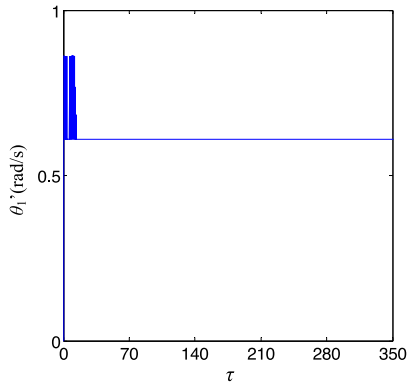

(c) $C = 10^8$ N

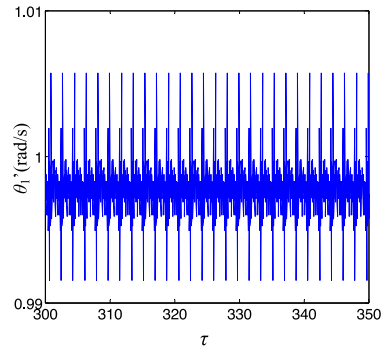

(d) $C = 8\times10^8$ N

Figure 5 Change of θ_1' under the different C

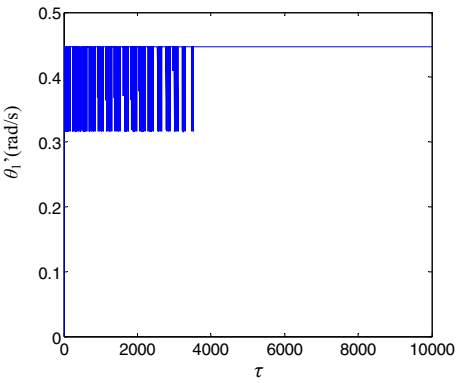

(a) H=1μm

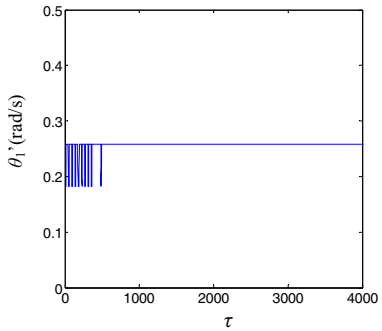

(b) H=1.5μm

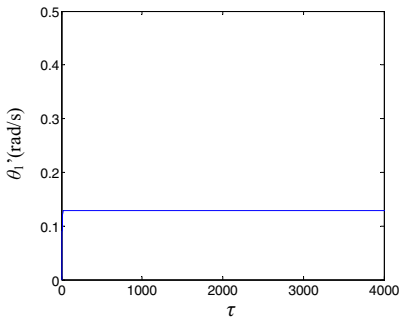

(c) H=2μm

Figure 6 Change of θ_1' under the different H

θ_1' continues to increase with the increases of C, which is seen in Figure 5c. When $C > 3 \times 10^8$ N/m, the rotation speed of the disc is the same as that of the shaft. With the increase of C, the rotation state of the disc is more stable. The increase of C is the increase of the contact stiffness, also is the increase of the interference force and the reduction of the looseness fault of the disc-shaft, therefore the rotation speed of the disc is getting more stable.

3.1.3 Influence of the Clearance of the Disc-Shaft

Let H is the clearance of the disc-shaft. Figure 6 shows the change of relative speed of the disc θ_1' under the different clearance of the disc-shaft H. From Figure 6, θ_1'

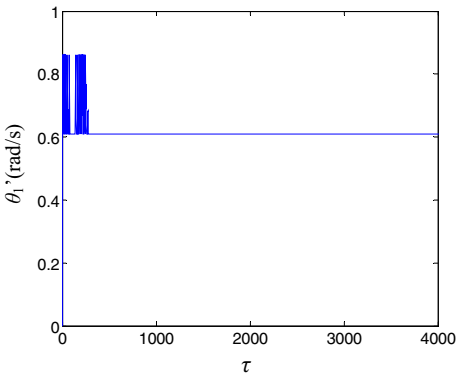

Figure 7 Change of θ_1' at $\xi_1 = 1/3$

gradually decreases with the increases of H. The reason is that the interference force of disc-shaft system gradually decreases with the increases of H. The influence of the interference force is consistent with the rotation speed of the shaft and the contact stiffness of disc-shaft.

3.1.4 Influence of Damping

Figure 7 is the change of θ_1' at $\xi_1 = 1/3$. Firstly, the influence of ξ_1 is analyzed. From Figure 7, under the condition of $\xi_2 = 2$ and $\xi_3 = 1/3 \times 10^9$, With the change of ξ_1, the simulation result demonstrates that the rotation state of the disc is almost constant, that is, the motion state of the disc is not sensitive to the change of ξ_1.

Next, the influence of ξ_2 is analyzed, under the condition of $\xi_1 = 1/3$ and $\xi_3 = 1/3 \times 10^9$, With the change of ξ_2, the simulation result shows that when $\xi_2 \geq 12$, θ_1' is always stable at 0.61. However, when $\xi_2 \leq 12$, the vibration amplitude of the disc becomes larger and larger, the rub-impact of the disc-shaft also gets more and more intense. The rotation speed of the disc is sharply increased from a certain value, which is lower than the rotational speed of the shaft, to fluctuation at the rotational speed of the shaft, and the sharp increase of rotating speed and serious vibration of the disc occur simultaneously. The serious change of the disc-shaft rubbing causes the frictional force to change drastically, thus causes θ_1' to fluctuate at θ_1'=1. Figure 8 shows that the change of motion state of the disc at $\xi_2 = 0.1$. From Figure 8, the amplitude of the disc is particularly large at this time, and is still increasing, this is obviously abnormal.

Finally, the influence of ξ_3 is analyzed under the conditions of $\xi_1 = 1/3$ and $\xi_2 = 2$. Figure 9 shows the change of θ_1' with ξ_3. The simulation result shows that the relative speed of the disc θ_1' gradually decreases with the increase of ξ_3. When ξ_3 is smaller, θ_1' decreased rapidly, and when

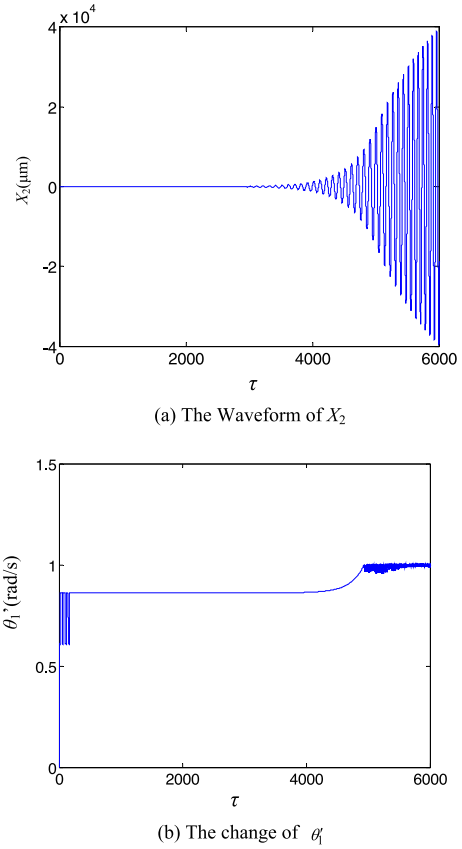

Figure 8 Change of motion state of the disc at $\xi_2 = 0.1$

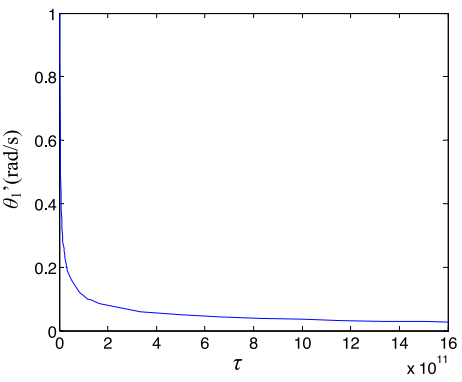

Figure 9 Change of θ_1' with ξ_3

ξ_3 is larger, θ_1' decreased slowly. The bigger the rotational damping is, the lower the rotating speed of the disc is.

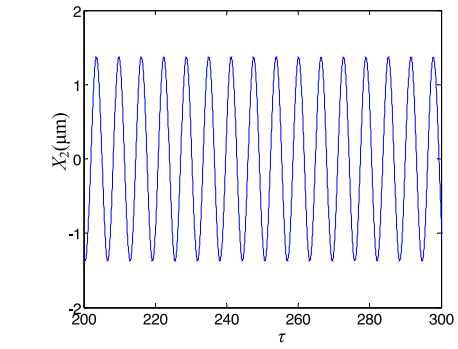

(a) The waveform of X_2

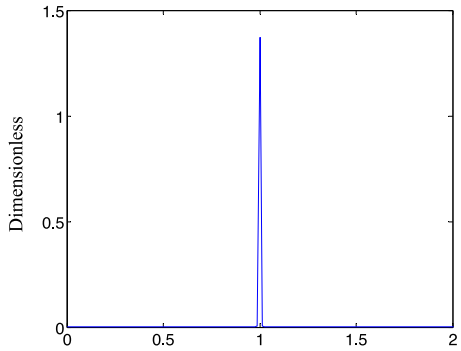

(b) The spectrum of X_2

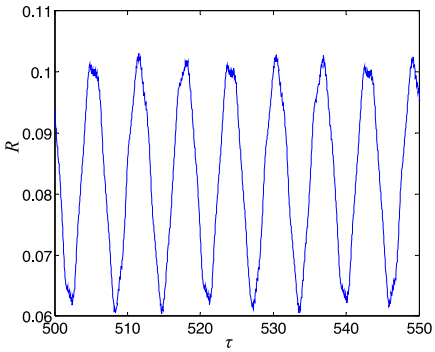

(c) The waveform of R

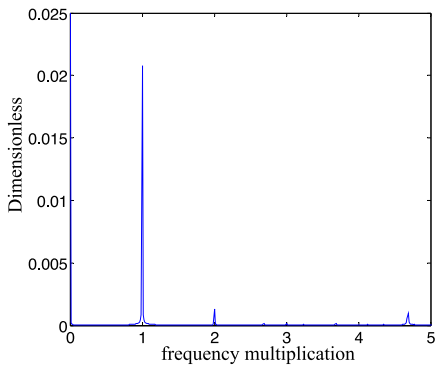

(d) The spectrum of R

Figure 10 Time-frequency characteristics of the disc-shaft at the same speed

3.2 Time-Frequency Characteristic Analysis

Figure 10 shows that the time-frequency characteristics of the disc-shaft when the rotation speed of the disc is the same as that of the shaft. From Figure 10b, the spectrum of X_2, i.e., in the horizon direction, is mainly composed of one frequency component. However, there is a process of collision between the disc and the shaft, and the frequency components of the disc-shaft collision should occur in the spectrum. The disc-shaft displacement difference R is a parameter that directly describes the process of the disc-shaft collision. From Figure 10d, one frequency multiplication is its main component in the collision frequency, and the amplitude of other frequency components are extremely weak compared with that in the X_2 spectrum, therefore the collision frequency of the disc-shaft is not found in the spectrum of X_2.

Figure 11 shows that the time-frequency characteristics of the disc in the x-direction and the time-frequency characteristics of the disc-shaft displacement difference R when $\theta_1' = 0.86$. From Figure 11b, the rotating frequency component of the disc and the rotating frequency component of the shaft the spectrum are both in the spectrum of X_2. The collision frequency component also doesn't occur in the spectrum of X_2. Since the rotating frequency component of the disc and the rotating frequency component of the shaft are close, the beat vibration of the disc occurs in the waveform of X_2, which is seen in Figure 11a. The periodic similar beat vibration also occurs in the waveform of the displacement difference of the disc-shaft. The result shows that the displacement difference of the disc-shaft has a causal relationship with the vibration of X_2. From Figure 11d, the spectrum of R is composed of a few low frequency multiplication components and a few weak high frequency components. Similarly, because the amplitude of the collision frequency component is very small, the collision frequency component is also not found in the X_2 spectrum.

Figure 12 shows that the time-frequency characteristics of the disc in the x-direction and the time-frequency characteristics of the disc-shaft displacement difference R when $\theta_1' = 0.42$. From Figure 12b, the rotating frequency component of the disc and the rotating frequency component of the shaft the spectrum are both in the spectrum of X_2. The collision frequency component also doesn't occur in the spectrum of X_2. From Figure 12d, the spectrum of R is composed of one multiplication component. A few weak low frequency multiplication components and a few weak high frequency components also occur in the spectrum of R. Similarly, because the amplitude of the collision frequency component is very small, the collision frequency component is also not found in Figure 12b.

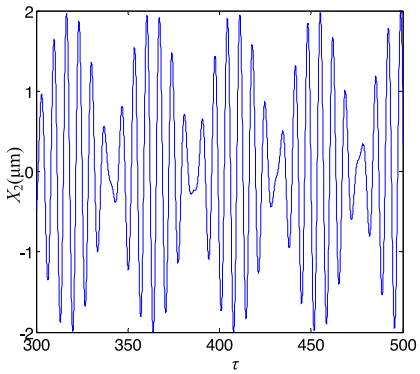

(a) The waveform of X_2

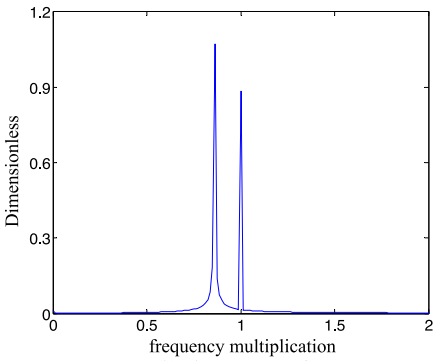

(b) The spectrum of X_2

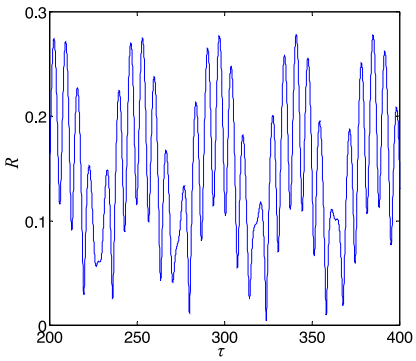

(c) The waveform of R

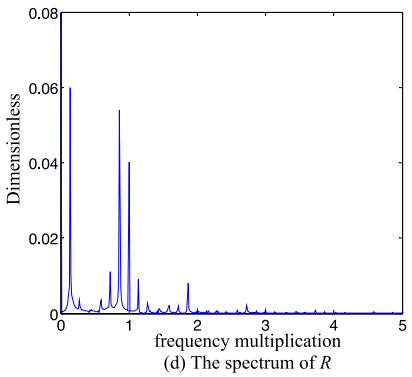

(d) The spectrum of R

Figure 11 Time-frequency analysis when $\theta_1' = 0.86$

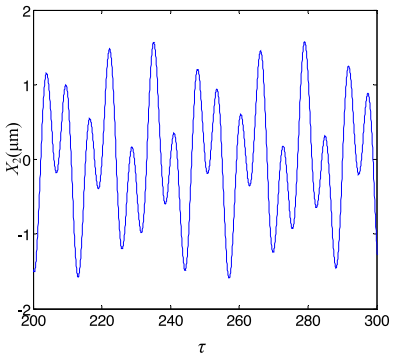

(a) The waveform of X_2

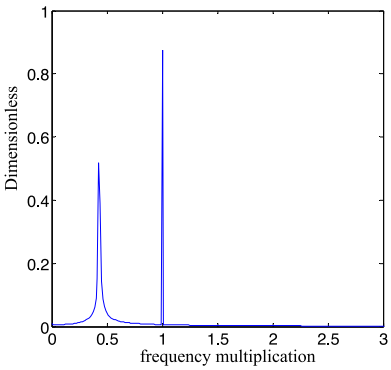

(b) The spectrum of X_2

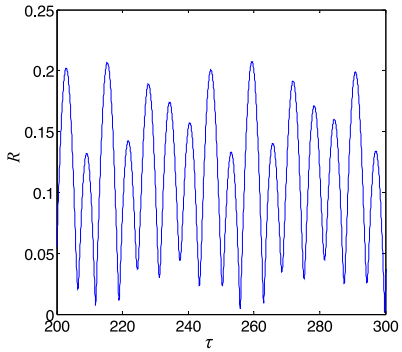

(c) The Waveform of R

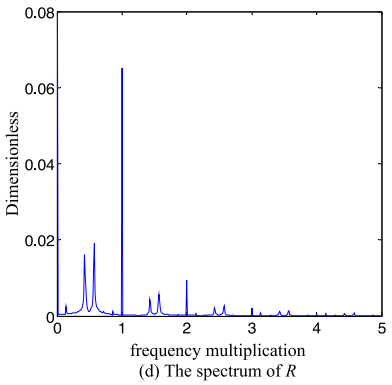

(d) The spectrum of R

Figure 12 Time-frequency characteristics when $\theta_1' = 0.42$

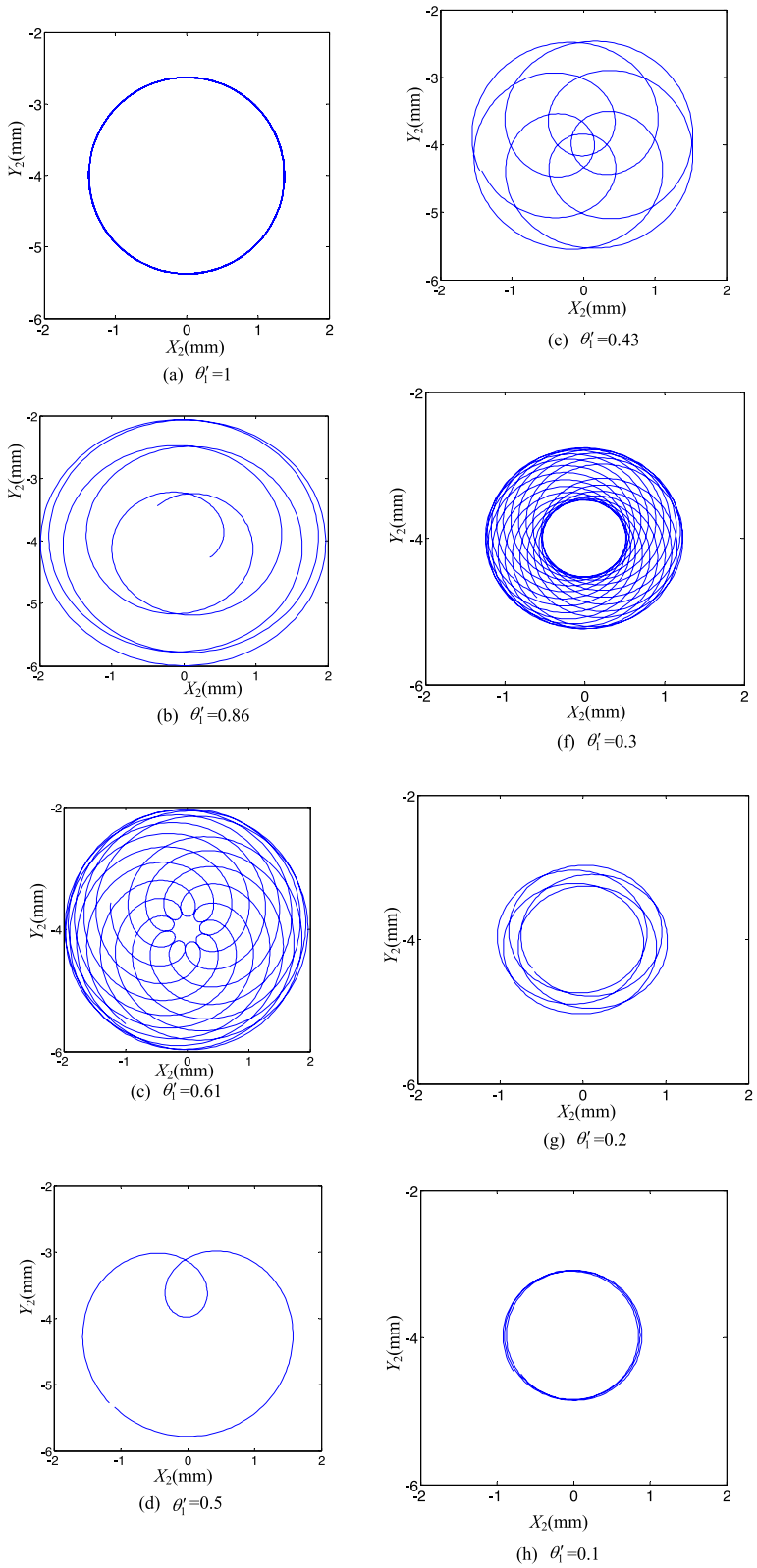

Figure 13 Trajectory of the disc under the different θ_1'

3.3 Motion Trajectory

Figure 13 shows the trajectory of the disc under the different θ_1'. From Figure 13, With the decreases of θ_1', the trajectory of the disc changes from circle-shape to inner eight-shape, and then return to circle-shape. In the inner eight-shape, the inner ring first gradually becomes smaller and then gradually becomes larger, the outer ring is still getting smaller. The appearance of the inner eight-shape is caused by the difference of θ_1'.

The reason why the outer ring has been getting smaller is that the centrifugal force is getting smaller due to the smaller and smaller relative speed of the disc-shaft θ_1'.

4 Experimental Research

The experimental system is composed of ZT-3 rotor test bench, Bentley displacement sensor and MULLER-BBM sampling system. Figure 14 is the ZT-3 rotor test bench. The ZT-3 rotor test bench consists of the power output system and the rotor system with loose disc. The flexible coupling is used as the demarcation point, the right half part of demarcation point is the power output system, which consists of motor, joint coupling, shaft, bearing seat, flexible coupling and phase bonder. The right side of the flexible coupling is connected to a shaft with a length of 320 mm, and the left side of the flexible coupling is connected to a shaft with a length of 500 mm. Both ends of the shaft are supported by the sliding bearings. In order to ensure the accuracy of the experimental results of the rotor system with loose disc, the flexible coupling is used to make the power output system only output torque, not horizontal or vertical vibration. The phase bonder is used to measure the rotational frequency of the shaft by an eddy current sensor. The motor in the experiment is a DC motor with the output power of 250 W. The speed controller is used to realize stepless speed in the range of 0−10000 r / min. The left half part of the demarcation point is a rotor system with loose disc, which consists of a rotating shaft, two bearing seats, and a disc. The diameter of the shaft is 9.5 mm, the mass of the disc is 0.612 kg, the outer diameter of the disc is 76.2 mm, and the distance between the centers of the two bearing seats is 422 mm.

Figure 15 Structure of the loose disc

This experiment is used to analyze the vibration characteristics of the rotor system with loose disc. Figure 15 is the structure of the loose disc, which consists of the

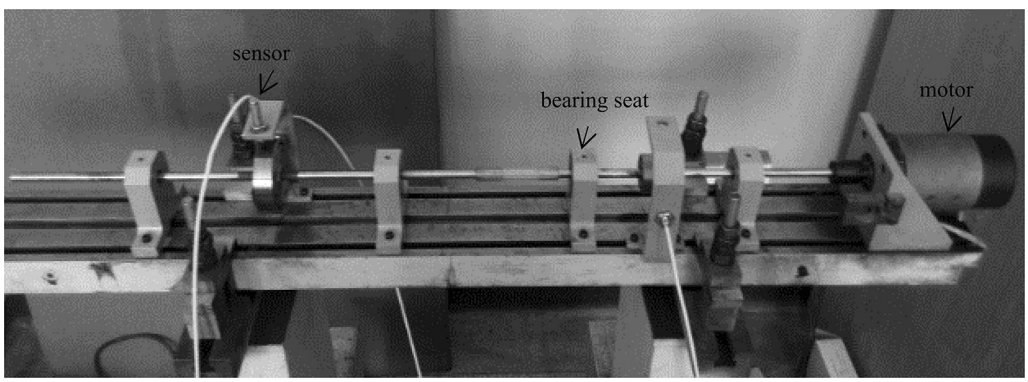

Figure 14 ZT-3 rotor test bench

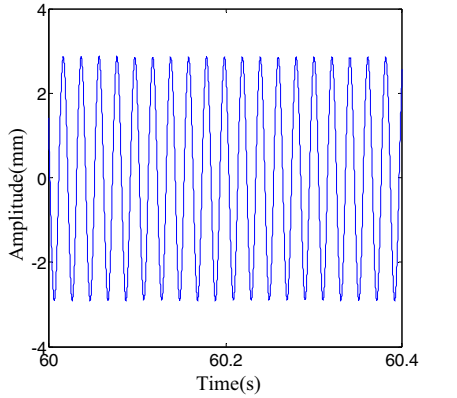

(a) Waveform

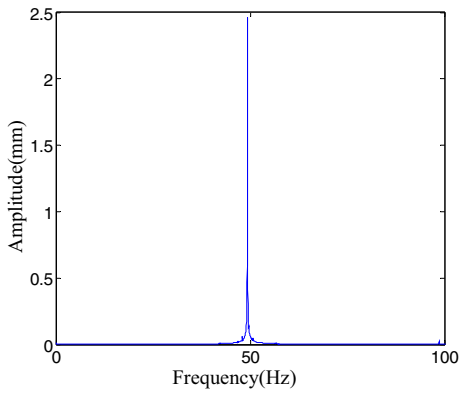

(b) Spectrum

Figure 16 Waveform and spectrum in the *x*-direction when the disc and the shaft is at the same speed

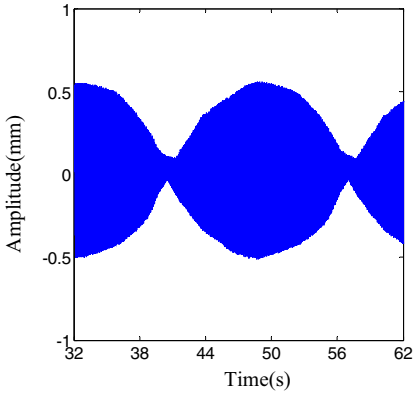

(a) Waveform

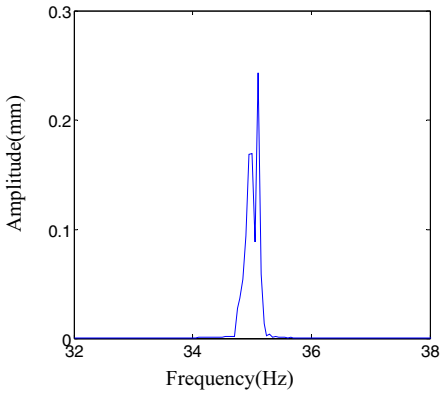

(b) Spectrum

Figure 17 Waveform and spectrum in the *x*-direction when the speed of the disc and the speed of the shaft is close

inner ring and the outer ring. These two parts are assembled together by a cone surface, and the pressure is provided by the screw thread. When the screw thread rotates clockwise, the inner ring and the outer ring are extruded by the cone surface contact, so that the diameter of the inner ring reduces. Therefore, the screw thread is only turned clockwise to fix the disc on the shaft, then turned counterclockwise, thus the clearance can be generated between the disc and the shaft.

4.1 Analysis of the Spectrum

Figure 16 shows that the waveform and spectrum in the x-direction when the disc and the shaft is at the same speed. Figure 17 shows that the waveform and spectrum in the x-direction when the speed of the disc and the speed of the shaft is close. Figure 18 shows that the waveform and spectrum in the x-direction when the disc and the shaft have a large difference in rotation speed. From Figure 16, when the disc and the shaft is at the same speed, the collision frequency is mainly composed of one frequency multiplication component. From Figure 18, when the disc and the shaft have a large difference in rotation speed, compared with Figure 16, except for one frequency multiplication component in the collision frequency, a few weak high frequency multiplication components and a few weak low frequency multiplication components also occur in the collision frequency. From Figure 17, when the speed of the disc and the speed of the shaft is close, the vibration of the disc occurs a beat vibration, the collision frequency is mainly composed of a few low frequency components. The experimental results are consistent with the simulation results.

4.2 Analysis of Motion Trajectory

Figure 19 shows that the trajectory of the disc under the different θ_1'. When the disc and the shaft is at the same speed, the trajectory of the disc is basically a circle-shape. With the decreases of θ_1', the trajectory changes from circle-shape to inner eight-shape, and then return to circle-shape. In the inner eight-shape, the inner ring first

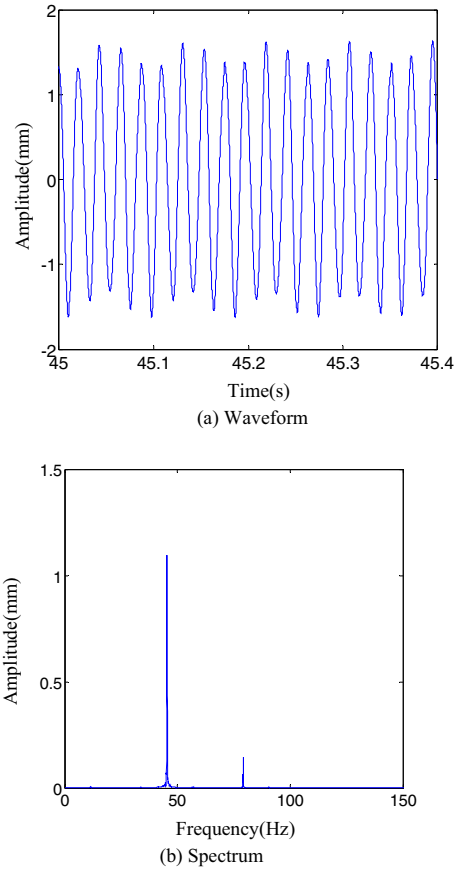

Figure 18 Waveform and spectrum in the *x*-direction when the disc and the shaft have a large difference in rotation speed

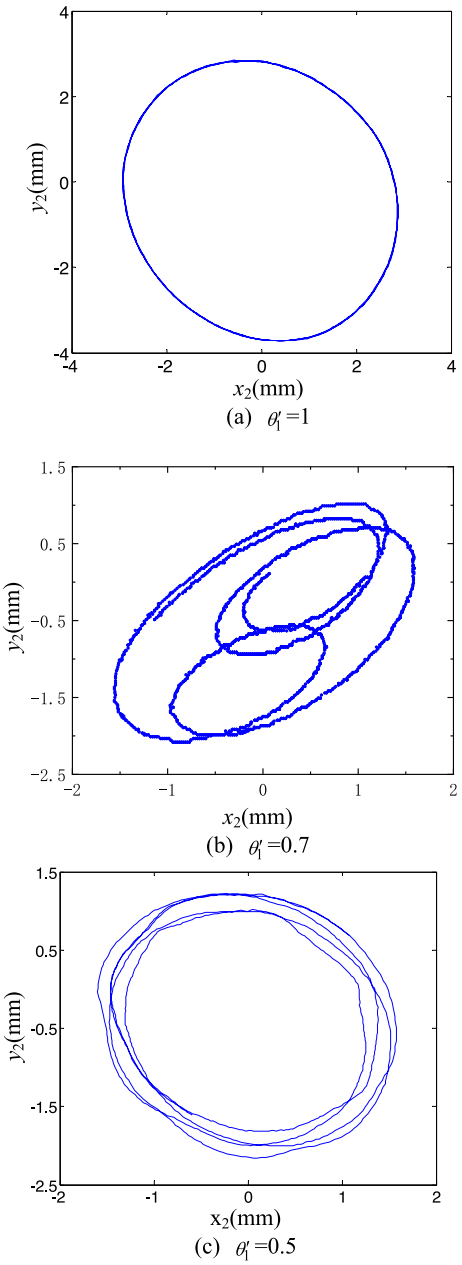

Figure 19 Trajectory of the disc under the different θ_1'

gradually becomes smaller and then gradually becomes larger, and the outer ring is still getting smaller. the experimental results are also consistent with the simulation results. The experiment results show that the simulation model is very reasonable.

5 Conclusions

A dynamic contact model of the rotor system with loose disc is proposed based on the contact model of the disc-shaft system with the microscopic surface topography. The influences of Ω, C, H, ξ_2 and ξ_3 on the motion state of the disc are discussed. The time-frequency characteristics of the disc and the motion trajectory of the disc are discussed. The experiment results verified the effectiveness of the proposed model. The obtained conclusions are as follows.

(1) The rotation speed of the shaft, the contact stiffness, the clearance, the damping of the disc, and the rotational damping all have an influence on the motion state of the disc. Compared with the rotor system with a loose disc caused by the clearance fit, The variation of vibration characteristics of the proposed model is smaller and more stable. The rotor system with slight fault is more stable and conforms to objective laws.

(2) The spectrum of the disc in the *x* direction is composed of the rotation frequency of the disc and the rotation frequency of the shaft. When the rotation speed of the disc and the rotation speed of the shaft

are same, the collision frequency is mainly composed of one frequency multiplication component. When the rotational speed of the disc and the rotation speed of the shaft is close, the beat vibration occurs in the x direction of the disc. Simultaneously, the periodical similar beat vibration phenomenon also occurs in the waveform of the disc-shaft displacement difference. The collision frequency is mainly composed of low frequency multiplication components and weak high frequency multiplication components. When the disc and the shaft have a large difference in rotation speed, the collision frequency is mainly composed of one frequency multiplication component, a few weak high frequency multiplication components and a few weak low frequency multiplication components.

(3) With the decrease of the relative rotation speed of the disc, the trajectory of the disc changes from changes from circle-shape to inner eight-shape, and then return to circle-shape. In the inner eight-shape, the inner ring first gradually becomes smaller and then gradually becomes larger, and the outer ring is still getting smaller. The appearance of the inner eight-shape is caused by difference in the speed between the disc and the shaft. With the rotating speed of the disc is getting lower and lower, the centrifugal force provided by the disc is getting smaller and smaller, and the outer ring of inner eight-shape is getting smaller.

Acknowledgements
Not applicable.

Authors' Information
Zhi-Nong Li, born in 1966, is currently a professor at *Key Laboratory of Nondestructive Testing*, *Ministry of Education, Nanchang Hangkong University, China.* He received his PhD degree from *Zhejiang University, China,* in 2003. His research interests include intelligent detection and signal processing, mechanical fault diagnosis.
Fang Qiao, born in 1995, is currently a graduate student at *Nanchang Hangkong University, China.*
Wen-Xiu Lu, born in 1974, is currently an associate professor at *Tsinghua university, China*. He received his PhD degree from *Tsinghua University, China,* in 2002.
Jie liu,born in1991, is a graduate student at *Nanchang Hangkong University,* China, in 2018.
Dong Wang, born in 1984, is currently an associate professor at *State Key Laboratory of Mechanical Systems and Vibration, Shanghai Jiao tong University, China.* He received his PhD degree from *City University of Hong Kong, China,* in 2015.
Fu-Lei Chu, born in 1959, is a professor at *Tsinghua University, China.* He received his PhD degree from *Southampton university, England,* in 1993.

Authors Contributions
ZL were in charge of the proposed model; FQ and JL wrote the manuscript; WL, DW and FC were in charge of the experiment. All authors read and approved the final manuscript.

Funding
Supported by National Natural Science Foundation of China (Grant Nos. 51675258, 51875301, 51265039), State Key Laboratory of Mechanical System and Vibration of China (Grant No. MSV201914), and Laboratory of Science and Technology on Integrated Logistics Support, National University of Defense Technology of China (Grant No. 6142003190210).

Competing Interests
The authors declare no competing financial interests.

Author Details
[1]Key Laboratory of Nondestructive Testing, Ministry of Education, Nanchang Hangkong University, Nanchang 330063, China. [2]Laboratory of Science and Technology on Integrated Logistics Support, National University of Defense Technology, Changsha 410073, China. [3]Department of Mechanical Engineering, Tsinghua University, Beijing 100084, China. [4]State Key Laboratory of Mechanical Systems and Vibration, Shanghai Jiao Tong University, Shanghai 200240, China.

Received: 28 May 2020 Revised: 14 March 2021 Accepted: 8 April 2022
Published online: 11 June 2022

References

[1] H Ma, Z Zhang, X Y Tai, et al. Dynamic characteristic analysis of a rotor system with pedestal looseness under two load case. *Proceedings of the CSEE*, 2012, 32(26): 132–137+158.
[2] C Y Sun, R Yang, Y S Chen, et al. Modeling and experiment verification of a casing-dual-rotor high-dimensional system. *Journal of Vibration and Shock*, 2018, 37(18): 152–157 (In Chinese).
[3] J Zhang, B C Wen. A study of frequency characteristics of rotor system with pedestal looseness at two supports. *China Mechanical Engineering*, 2008(1): 68–71 (In Chinese).
[4] Y J Lu, Z H Ren, H Hou, et al. Study on looseness and impact-rub coupling faults of vertical dual-disc over-hung rotor-bearing system. *Journal of Vibration, Measurement & Diagnosis*, 2007(2): 102–107+169.
[5] J Mian, J G Wu, X S Peng, et al. Nonlinearity measure based assessment method for pedestal looseness of bearing-rotor systems. *Journal of Sound and Vibration*, 2017, 411: 232–246.
[6] Z Y Qin, Q K Han, F L Chu. Bolt loosening at rotating joint interface and its influence on rotor dynamics. *Engineering Failure Analysis*, 2016, 59.
[7] Z Y Qin, F L Chu. Numerical studies on time-varying stiffness of disk-drum type rotor with bolt loosening. *Journal of Physics: Conference Series*, 2015, 628(1).
[8] Y Liu, Z Y Xue, L Jia, et al. Response characteristics of looseness-rubbing coupling fault in rotor-sliding bearing system. *Mathematical Problems in Engineering*, 2017, 2017(PT.11): 1–10.
[9] Z P Li, Y G Luo, H L Yao, et al. Dynamics and fault characteristics of rotor-bearing system with pedestal looseness. *Journal of Northeastern University* (*Natural Science*), 2002, 23(11): 1048–1051 (In Chinese).
[10] Y Liu, X Y Tai, H Ma, et al. Looseness-rubbing coupling fault of dual-disk three-support rotor-bearing system. *Journal of Aerospace Power*, 2013, 28(5): 977–982 (In Chinese).
[11] H F Wang, G Chen. Modeling for whole missile turbofan engine vibration with support looseness fault and characteristics of casing response. *Journal of Aerospace Power*, 2015, 30(3): 627–638 (In Chinese).
[12] H Yu, Y H Ma, S Xiao, et al. Mechanical and dynamic characteristics of bearing with looseness on high-speed flexible rotor. *Journal of Beijing University of Aeronautics and Astronautics*, 2017, 43(8): 1677–1683 (In Chinese).
[13] G Chen. Nonlinear dynamics of unbalance-looseness coupling fults of rotor-ball bearing-stator coupling system. *Chinese Journal of Mechanical Engineering*, 2008, 44(3): 82–88 (In Chinese).
[14] J Zhang, H Li, B C Wen. On the pedestal looseness of dynamic oil film-rotor system. *Journal of Northeastern University* (*Natural Science*), 2003, 24(10): 880–880 (In Chinese).
[15] Q S Cao, Y M Huang. An improved genetic algorithm for pedestal looseness parameter identification in rotor-bearing systems. *Journal of Vibration, Measurement & Diagnosis*, 2018, 38(3): 446–453.
[16] H Z Xu, N F Wang, D X Jiang. Bearing pedestal looseness dynamic model of dual rotor system and fault feature. *Journal of Aerospace Power*, 2016, 31(11): 2781–2794 (In Chinese).

[17] Y Yang, Y R Yang, D Q Cao, et al. Response evaluation of imbalance-rub-pedestal looseness coupling fault on a geometrically nonlinear rotor system. *Mechanical Systems and Signal Processing*, 2019, 18: 423–442.
[18] Q S Cao, Q Xiang, G L Xiong. Incremental harmonic balance method for the study of support looseness fault's characteristics. *Journal of Mechanical Strength*, 2015(6): 999–1004 (In Chinese).
[19] H R Cao, F Shi, Y M Li, et al. Vibration and stability analysis of rotor-bearing-pedestal system due to clearance fit. *Mechanical Systems and Signal Processing*, 2019, 133: 106275.
[20] M Behzad, M Asayesh. Vibration analysis of rotating shaft with loose disk. *IJE Transactions B: Applications,* 2002, 15(4): 385–393.
[21] M Behzad, M Asayesh. Numerical and experimental investigation of the vibration of rotors with loose discs. *Proc. IMechE Part C. Mechanical Engineering Science*, 2010, 224: 85–94.
[22] G X Yang, J L Xie, S X Zhou, et al. Research on the influence of axle design parameters on contact pressure between axle and hub. *Journal of the China Railway Society*, 2009, 31(3): 31–35 (In Chinese).
[23] J Liu, Z N Li, W X Luo. Effects of unsteady oil film force on rotor system with loose disk and shaft. *Journal of Vibration and Shock*, 2019, 38(17): 268–275 (In Chinese).
[24] Z N Li, J Liu, W X Luo, et al. Research on dynamic modeling and simulation of rotors with loose disc. *Journal of Mechanical Engineering*, 2020, 56(7): 60–71 (In Chinese).
[25] S H Wei, W X Lu. Analysis on vibration characteristics of disk-shaft system with loose fit. *Journal of Dynamics and Control*, 2018, 16(3): 244–249 (In Chinese).
[26] S H Wei, W X Lu, F L Chu. Speed characteristics of disk-shaft system with rotating part looseness. *Journal of Sound and Vibration*, 2020, 469.
[27] H Wang, K H Qin, D N Zhou. Nonlinear dynamic modeling of rotor system supported by angular contact ball bearings. *Mechanical Systems and Signal Processing*, 2017, 85: 16–40.
[28] H Zhang, X Zhang, N N He. Rotor dynamic analysis of small vehicle gasoline turbocharger in semi-floating bearings. *Journal of Beijing Institute of Technology*, 2011, 20(4): 502–508 (In Chinese).
[29] M F Liao, Y Li, M B Song, et al. Dynamics modeling and numerical analysis of rotor with elastic support/dry friction dampers. *Transactions of Nanjing University of Aeronautics and Astronautics*, 2018, 35(1): 69–83 (In Chinese).
[30] L Yang, S P Yang, J J Wang, et al. Nonlinear vibration analysis of locomotive rotor system. *Journal of Mechanical Engineering*, 2018, 54(18): 97–104 (In Chinese).